Electronic Supplementary Information

The Kinetics and Mechanism of Oxidation of Reduced Phosphovanadomolybdates by Molecular Oxygen: Theory and Experiment in Concert

Alexander M. Khenkin, Irena Efremenko, Jan M. L. Martin, and Ronny Neumann*
Department of Organic Chemistry, Weizmann Institute of Science, Rehovot, Israel 76100

Table S1. The volumetric determination of dioxygen consumption for $\mathbf{1}_{red1e}$, and $\mathbf{1}_{red2e}$.

Polyoxometalate	$[O_2]$, µmol
$\mathbf{1}_{red2e}$	50±5
$\mathbf{1}_{red1e}$	25±2

Conditions: [$\mathbf{1}_{red}$] = 100 µmol in 2 mL of acetonitrile under air, T = 25 °C. Reactions were carried out in a magnetically stirred 10 mL volumetric flask kept at 25° ±0.2 °C with an oil bath (room temperature was 24-25 °C) connected to a gas burette for measuring the volume of consumed oxygen. The combined head space above the reaction solution was ~10 mL. The experimental error was ~ 10%.

Table S2. Outer-sphere reactions of O_2 and its reduced species with $H_6PV_2Mo_{10}O_{40}$ and with $H_7PV_2Mo_{10}O_{40}$ in gas phase and in acetonitrile at 298 K

	Gas phase				Acetonitrile			
	O_2	HO_2	H_2O_2	OH[a]	O_2	HO_2	H_2O_2	OH[a]
				$H_6PV_2Mo_{10}O_{40}$				
PT	167.2	117.3	121.7	129.0	69.6	28.2	31.7	28.7
ET	165.7	233.5	149.8	135.7	45.6	130.3	41.7	4.6
CPET	20.1	-11.4	-10.2[a]	-45.1	16.9	-10.3	-12.2[a]	-44.8
				$H_7PV_2Mo_{10}O_{40}$				
PT	171.6	121.7	126.1	133.4	72.2	30.8	34.3	31.3
ET	162.7	230.5	146.8	132.7	42.5	127.2	38.6	1.5
CPET	17	-14.5	-13.3[a]	-48.2	13.4	-13.8	-15.7[a]	-48.3

[a] H_3O_2 dissociates to H_2O and OH.

Table S3. Calculated stability of Mo-O-V and V-O-V reactive sites in acetonitrile at 298 K with respect to the corresponding intact Keggin structures. See Figure S9 for some typical defect structures with H_2O.

	$H_5PV_2Mo_{10}O_{40}$	$[H_5PV_2Mo_{10}O_{40}]^{1-}$	$H_6PV_2Mo_{10}O_{40}$	$[H_6PV_2Mo_{10}O_{40}]^{1-}$	$H_7PV_2Mo_{10}O_{40}$
V CUS (1,2)	20.54	19.58	22.28	17.64	18.64
Mo CUS (1,2)	16.50	17.85	16.93	13.75	15.32
Mo CUS (1,11)	16.25	14.10	14.35	15.08	15.54
V CUS (1,2)-H_2O	8.75	8.24	11.20	9.54	19.52
Mo CUS (1,2)-H_2O	7.59	9.73	7.42	5.01	14.27
Mo CUS (1,11)-H_2O	8.62	6.96	6.85	8.03	13.22

Table S4. Typical O_2 coordination modes to polyoxometalates isomers and their characteristics: ΔG_{298}, kcal/mol with respect to the intact polyoxometalate (defect structure), O-O and M-O bond distances (d, Å), O-O bond streching vibrational frequency (ν_{O-O}, cm^{-1}) and Atomic Polar Tensor (APT) charges on oxygen atoms.

			$H_5PV_2Mo_{10}O_{40}^-$	$H_6PV_2Mo_{10}O_{40}$	$H_6PV_2Mo_{10}O_{40}^-$	$H_7PV_2Mo_{10}O_{40}$
η^2-Mo-O_2	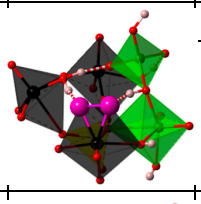	ΔG_{298}	21.1 (3.3)	22.7 (5.8)	2.1 (-11.7)	**7.3 (-8.0)**
		d_{O-O}	1.312	1.311	1.442	1.440
		ν_{O-O}	1180.3	1195.0	925.5	928.8
		d_{Mo-O}	2.148; 2.182	2.207; 2.189	1.986; 2.006	1.986; 2.011
		O-APT ch.	-0.217; -0.089	-0.207; -0.175	-0.366; -0.445	-0.349; -0.454
η^2-V-O_2	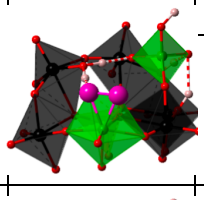	ΔG_{298}	15.9 (-3.7)	17.4 (-4.9)	4.4 (-13.2)	11.7 (-6.9)
		d_{O-O}	1.304	1.302	1.428	1.423
		ν_{O-O}	1203.1	1212.0	951.1	954.2
		d_{V-O}	2.024; 2.018	2.017; 2.014	1.903; 1.927	1.917; 1.851
		O-APT ch.	-0.180; -0.056	-0.152; -0.067	-0.325; -0.439	-0.259; -0.270
η^2-Mo-O_2 (1,11)	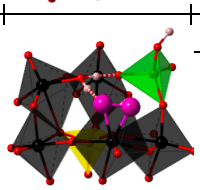	ΔG_{298}	17.8 (3.7)	20.0 (5.7)	2.0 (-13.0)	5.0 (-10.5)
		d_{O-O}	1.312	1.307	1.445	1.443
		ν_{O-O}	1184.0	1191.0	929.6	950.7
		d_{Mo-O}	2.148; 2.195	2.120; 2.201	1.972; 1.952	1.974; 1.948
		O-APT ch.	-0.206;-0.119	-0.177; -0.108	-0.358;-0.277	-0.344;-0.266
Mo-OO-V	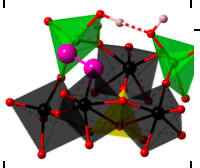	ΔG_{298}	34.9	39.5	20.6	24.2
		d_{O-O}	1.327	1.328	1.450	1.436
		ν_{O-O}	1106.6	1105.1	822.9	849.0
		d_{Mo-O}	2.219; 2.054	2.189; 2.045	1.995; 1.846	2.011; 1.828
		O-APT ch.	-0.166; -0.241	-0.149; -0.253	-0.390; -0.416	-0.339; -0.417
V-OO-V	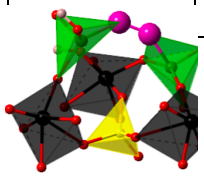	ΔG_{298}	39.5	41.8	30.6	26.4
		d_{O-O}	1.297	1.295	1.358	1.385
		ν_{O-O}	1200.8	1203.1	869.4	954.8
		d_{V-O}	1.992; 2.403	1.986; 2.416	1.871; 1.858	1.842; 1.870
		O-APT ch.	-0.099; -0.291	-0.083; -0.279	-0.341; -0.360	-0.423; -0.316
Mo-OO	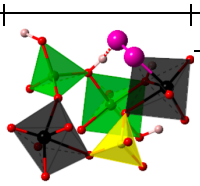	ΔG_{298}	22.6	27.5	20.5	22.8
		d_{O-O}	1.321	1.320	1.323	1.321
		ν_{O-O}	1152.9	1154.5	1127.8	1150.4
		d_{Mo-O}	2.205	2.196	2.201	2.206
		O-APT ch.	-0.142; -0.357	-0.128; -0.347	-0.055; -0.348	-0.116; -0.339
V-OO	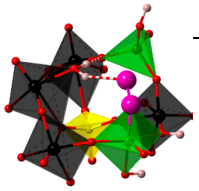	ΔG_{298}	21.2	26.4	Not found	Not found
		d_{O-O}	1.288	1.273		
		ν_{O-O}	1258.1	1263.8		
		d_{V-O}	1.972	1.943		
		O-APT ch.	0.313; -0.482	-0.016; -0.232		
Mo-OOH	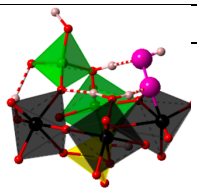	ΔG_{298}	25.1	26.8	6.6	13.9
		d_{O-O}	1.334	1.333	1.437	1.450
		ν_{O-O}	1133.5	1135.7	899.7	888.2
		d_{Mo-O}	2.315	2.311	1.983	1.985
		O-APT ch.	-0.014; -0.406	-0.025; -0.368	-0.209; -0.482	-0.353; -0.323
V-OOH	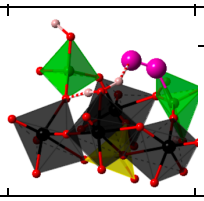	ΔG_{298}	29.5	Not found	15.0	25.5
		d_{O-O}	1.335		1.382	1.378
		ν_{O-O}	1113.8		1001.4	1017.3
		d_{V-O}	2.087		1.811	1.813
		O-APT ch.	0.117; -0.454		-0.145; -0.298	-0.096; -0.278

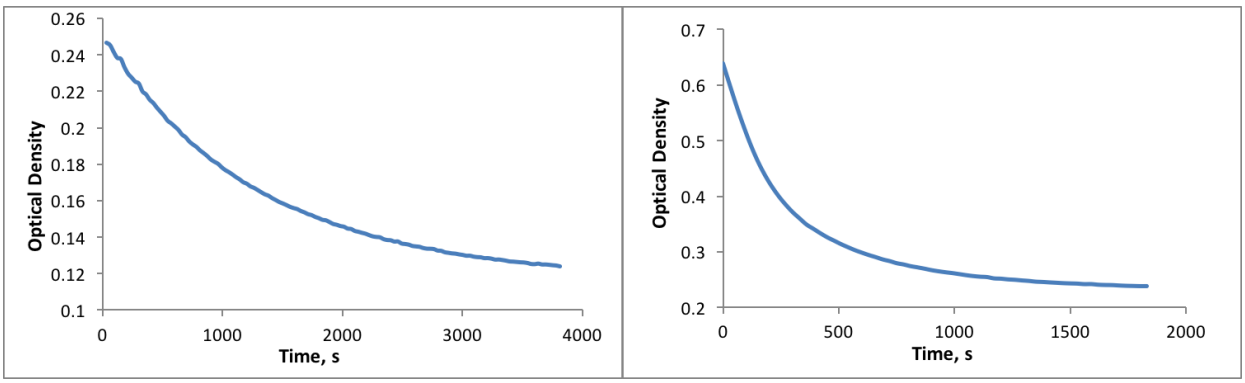

Figure S1. Exemplery kinetic profiles for the oxidation of 0.25 mM $\mathbf{1}_{red1e}$ (left) and 0.27 mM $\mathbf{1}_{red2e}$ (right) after reduction with H_2 followed decrease of absorbance at 750 nm. [$\mathbf{1}_{red1e}$] = 0.25 mM, in acetonitrile saturated with air at 25 °C.

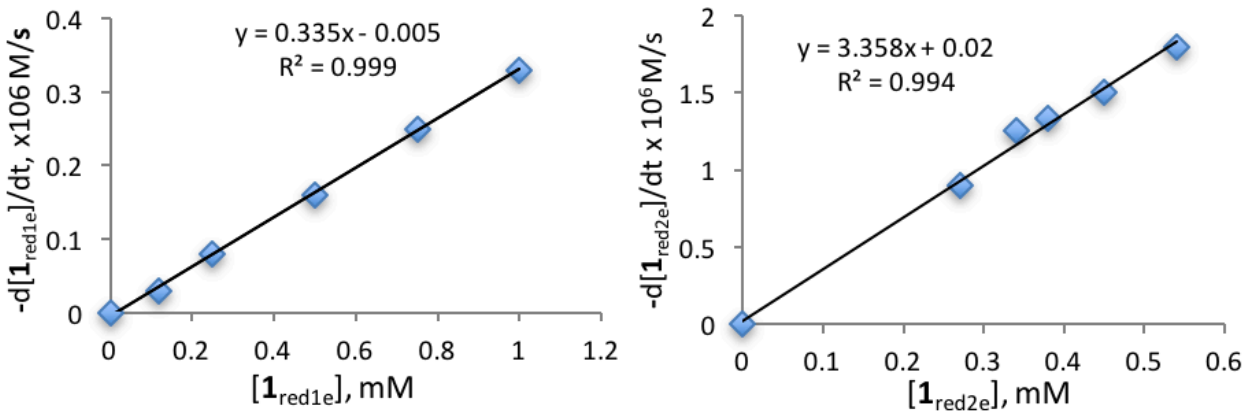

Figure S2. Dependence of initial rate (-d[$\mathbf{1}_{red}$]$_0$/dt) of the oxidation of [$\mathbf{1}_{red1e}$] (left) and [$\mathbf{1}_{red2e}$] (right) in acetonitrile at the initial O_2 concentration of 2.4 mM at 25 °C.

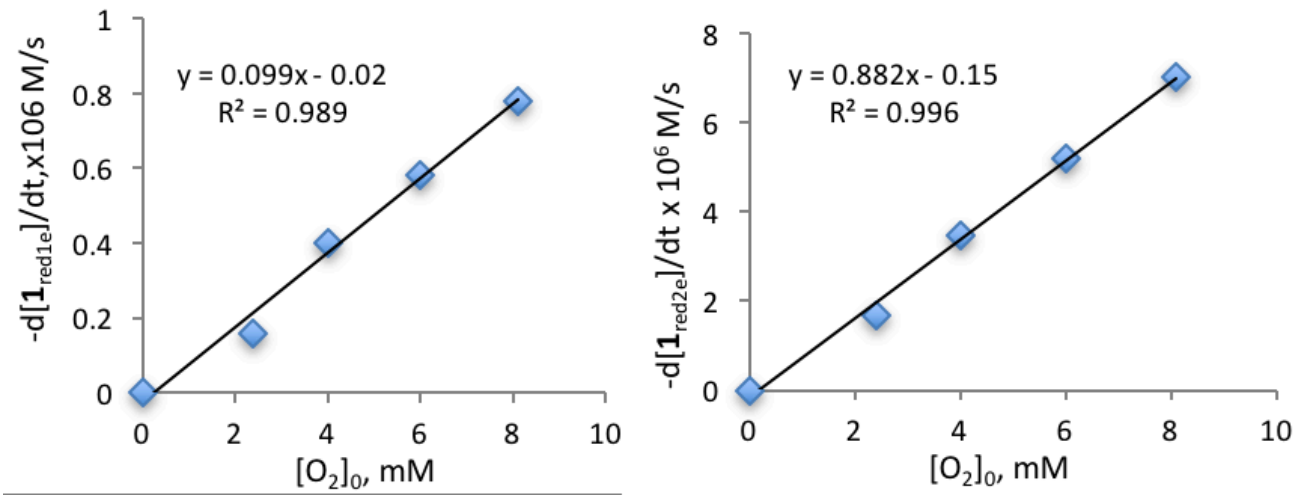

Figure S3. Dependence of the initial rate (-d[$\mathbf{1}_{red1e}$]$_0$/dt) of the oxidation of [$\mathbf{1}_{red1e}$] (0.5 mM) (left) and dependence of the initial rate (-d[$\mathbf{1}_{red2e}$]$_0$/dt) of the oxidation of [$\mathbf{1}_{red2e}$] (0.5 mM) (right) in acetonitrile on the initial concentration of O_2 [O_2]$_0$ at 25 °C.

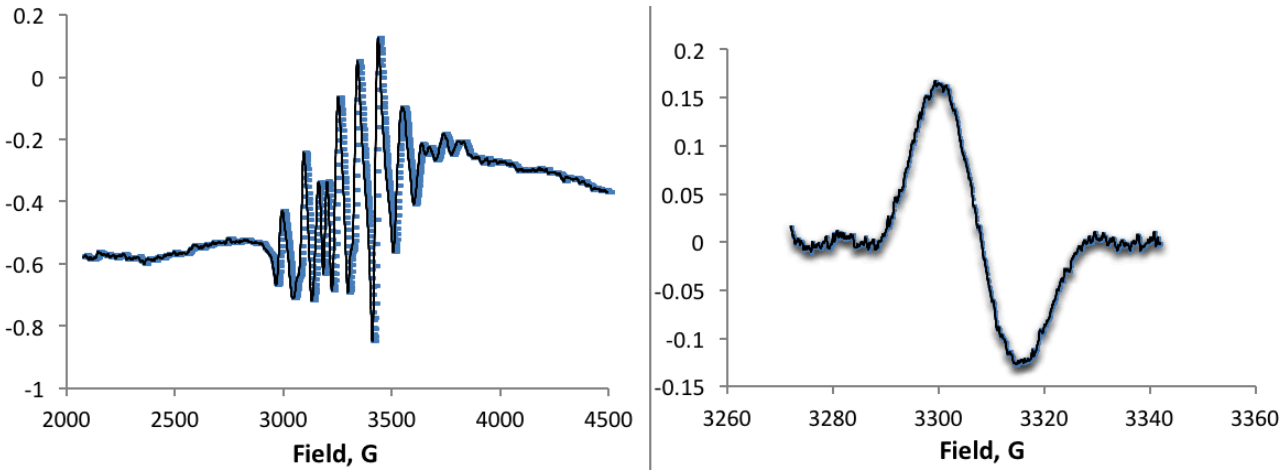

Figure S4. EPR Spectra. Left – 1 mM $H_5PV_2Mo_{10}O_{40}$ + 1 mM Ph_3P in acetonitrile at 25°C under Ar showing the contribution of V(IV) and Ph_3P•+. Right- g= 2.008 signal (zoom in) on the peak associable to Ph_3P•+.

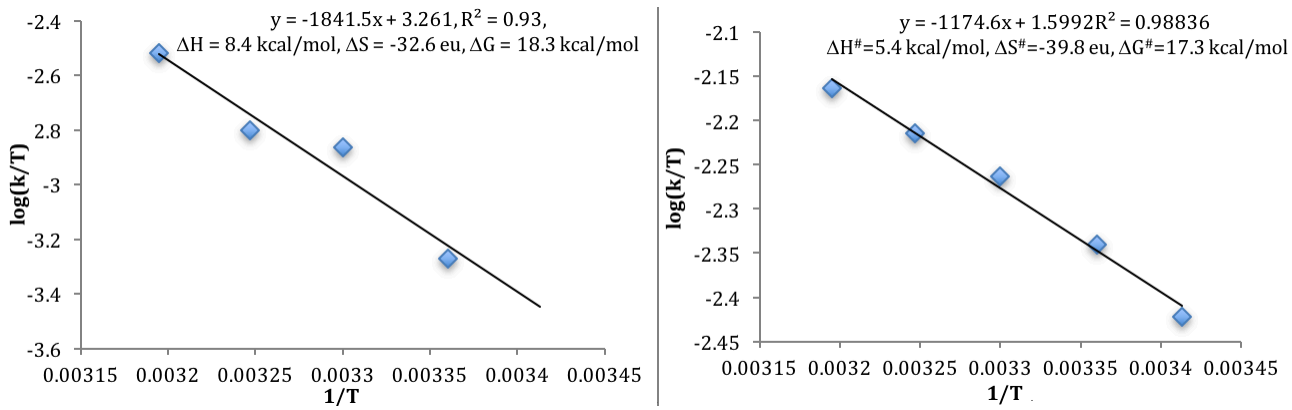

Figure S5. Eyring plot of reoxidation of $\mathbf{1}_{red1e}$ (left) and $\mathbf{1}_{red2e}$ (right) after reduction with H_2.[**1**] = 0.5 mM under air, in acetonitrile.

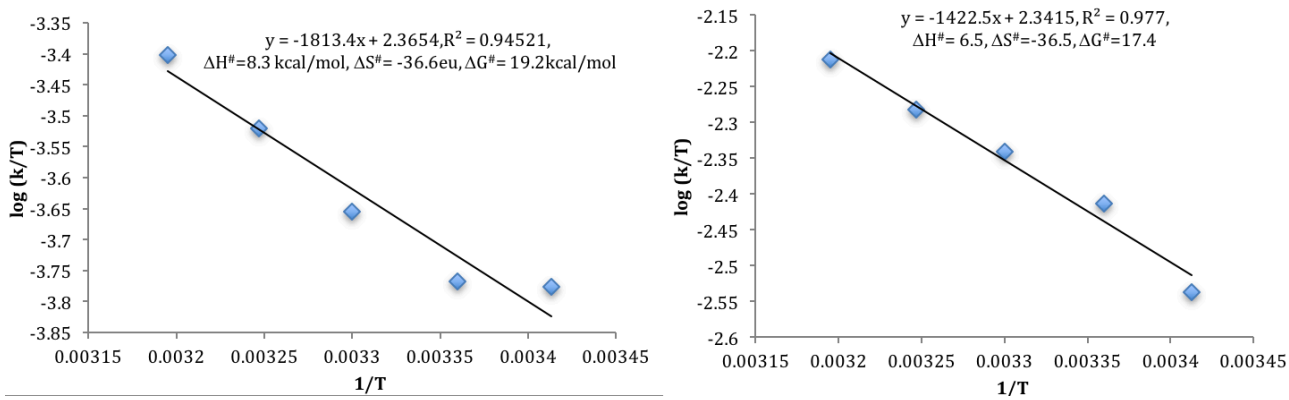

Figure S6. Eyring plot of reoxidation of $\mathbf{1}_{red1e}$ (left) and $\mathbf{1}_{red2e}$ (right) after reaction with Ph_3P at 70°C for 2 hours. [**1**] = 0.5 mM, [Ph3P] = 0.25 mM or 0.50 mM under air in acetonitrile.

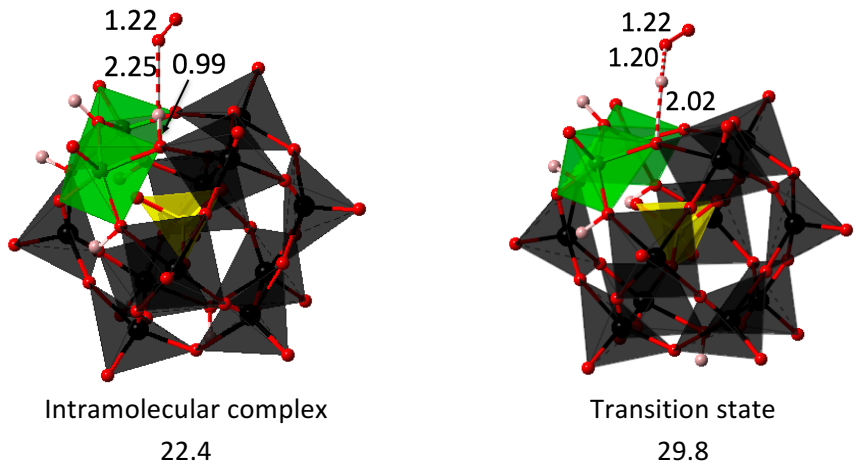

Figure S7. – Optimized structures of outer-sphere complexes $H_6PV_2Mo_{10}O_{40}$-O_2 and their calculated energies (ΔG_{298}, kcal/mol) in acetonitrile

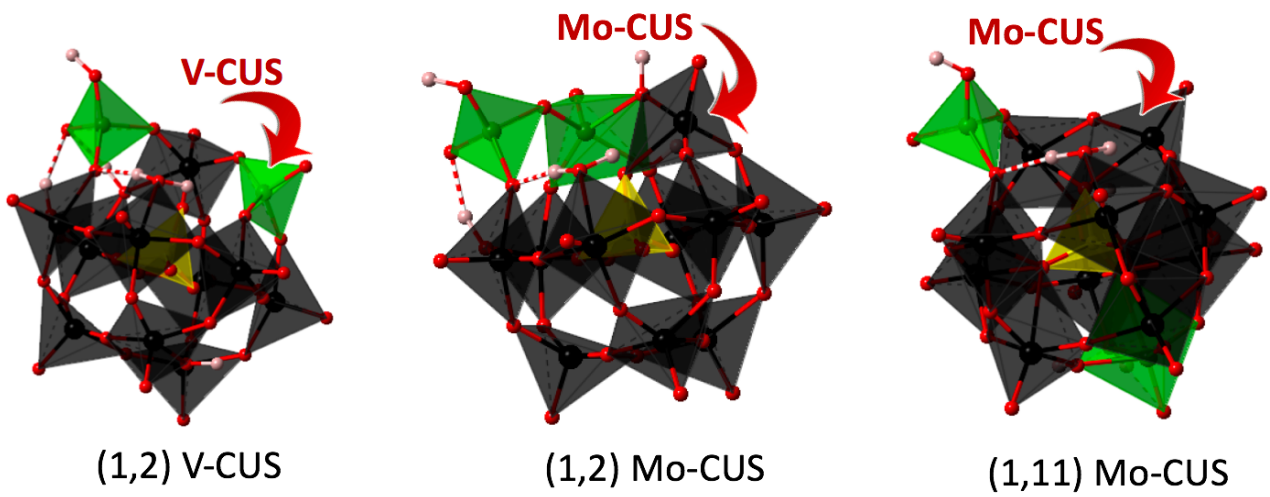

Figure S8. – Optimized structures of CUS species in Table 3

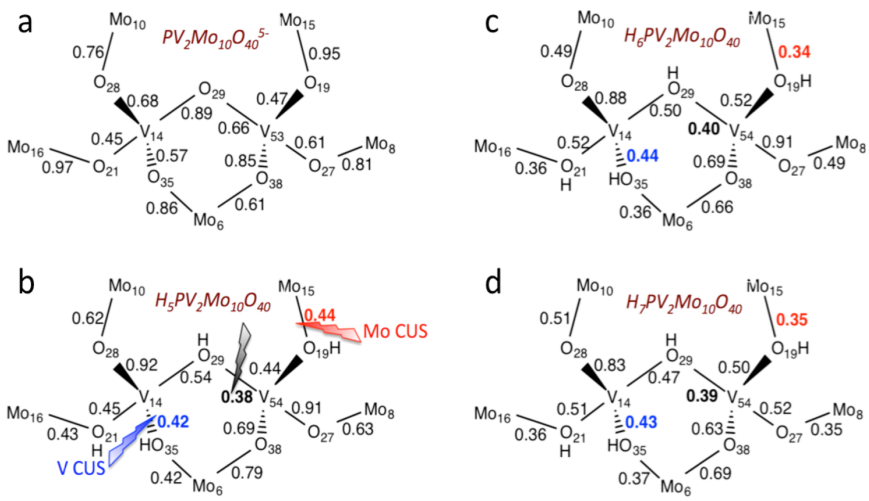

Figure S9. Wiberg bond indices for selected V-O and Mo-O bonds in (1,2) isomer of polyoxoanion $PV_2Mo_{10}O_{40}^{5-}$ (a), its protonated form $H_5PV_2Mo_{10}O_{40}$ (b) and in 1e- and 2e-reduced polyoxometalates $H_6PV_2Mo_{10}O_{40}$ (c) and $H_7PV_2Mo_{10}O_{40}$ (d).

Further explanation: Explicit consideration of protons is critically important for understanding of defect formation (a and b). One of the V-O–bonds, V_{53}-O_{29}, represents the weakest bridging bond in the $H_5PV_2Mo_{10}O_{40}$ (1,2) isomer. Breaking of this bond together with one of the other weak bonds, Mo_{15}-O_{19} or V_{14}-O_{35}, leads to Mo or V CUS, respectively. Decreased stabilization of the surrounding framework permits breaking of the bond connecting the V_{14} CUS atom with the central PO_4 tetrahedron and further destabilization of the Keggin structure: the V_{14}-O_i bond length in this structure is 2.54 Å, compared to 2.15 Å for the Mo_{15}-O_i distance in the structure with a Mo CUS, while the corresponding Wiberg bond orders are 0.14 and 0.30, respectively. That makes the V CUS species 4 kcal/mol higher in energy than its Mo CUS counterpart. Reduction of phosphovanadomolibdates strongly destabilizes Mo-O bonds making Mo CUS formation preferential, both kinetically and thermodynamically (c, d). Very similar results were found for the (1,11) isomer.

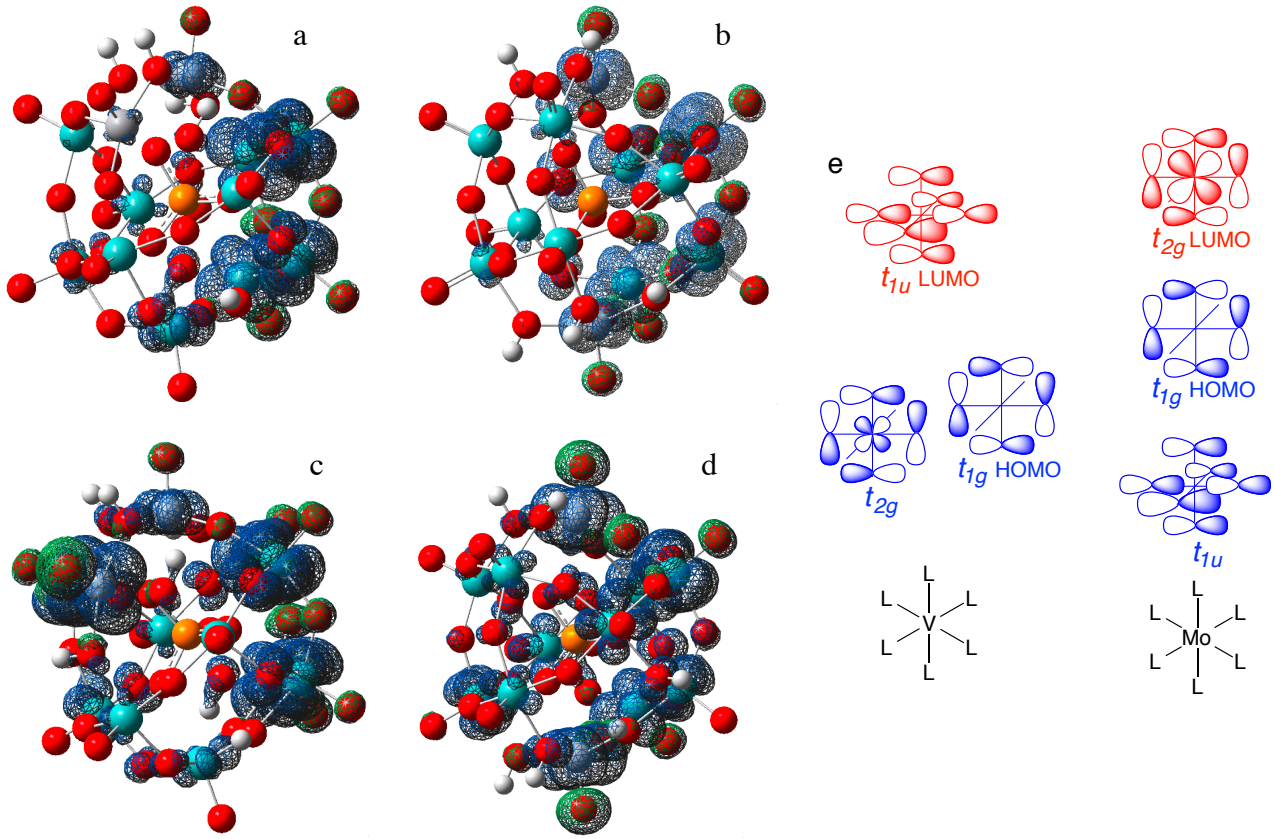

Figure S10. Spin density distribution in the (1,2) (a,c) and (1,11) (b,d) isomers of $\mathbf{1}_{red1e}$ (a,b) and $\mathbf{1}_{red2e}$ (c,d). Qualitative representation of the boundary orbitals of V^{5+} and Mo^{6+} in the octahedral crystal field of strong σ and π donor ligands and their relative energies (e).

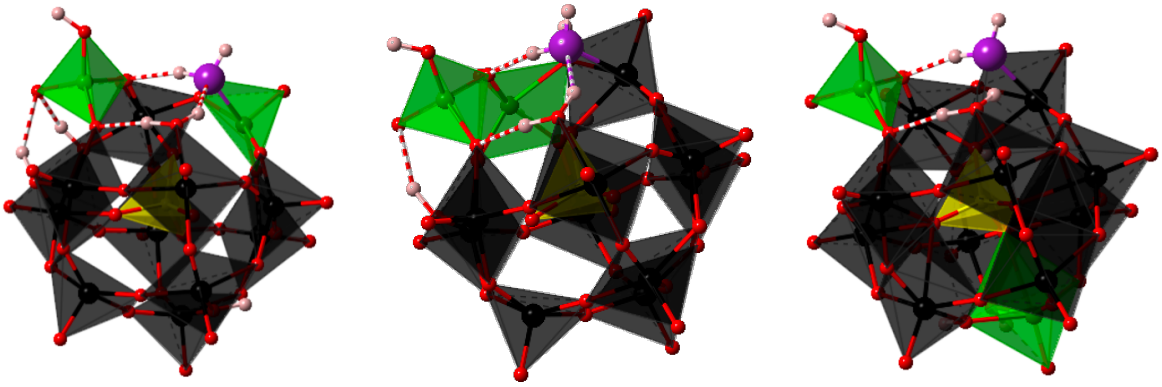

V CUS (1,2) -H_2O Mo CUS (1,2)-H_2O Mo CUS (1,11)-H_2O

Figure S11. Typical defect structures with CUS on V and on Mo atoms in presence of water. Large purple spheres distinguish O-atom of coordinated water.

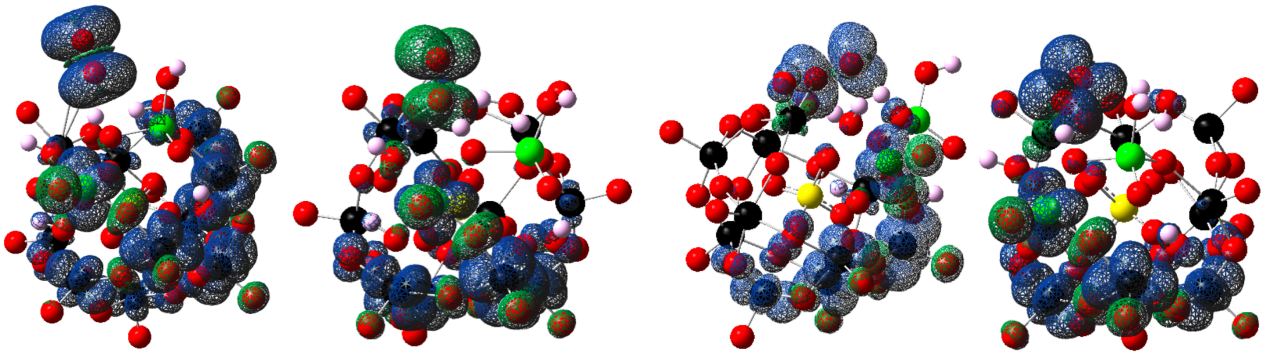

quintet M-OO OSS η^2 Mo-O_2 triplet Mo-OO triplet η^2 Mo-O_2

Figure S12. Spin density distribution in $\mathbf{1}_{red2e}$-O_2 complexes in different multiplicity states.